

Comparison of heritability estimates on resting state fMRI connectivity phenotypes using the ENIGMA analysis pipeline

Bhim M. Adhikari¹, Neda Jahanshad², Dinesh Shukla¹, David Glahn³, John Blangero⁴, Peter T. Fox⁵, Richard C. Reynolds⁶, Robert W. Cox⁶, Els Fieremans⁷, Jelle Veraart⁷, Dmitry S. Novikov⁷, Thomas E. Nichols⁸, L. Elliot Hong¹, Paul M. Thompson², Peter Kochunov*¹

1. Maryland Psychiatric Research Center, Department of Psychiatry, University of Maryland School of Medicine, Baltimore, MD, USA
2. Imaging Genetics Center, Stevens Institute for Neuroimaging & Informatics, Keck School of Medicine of USC, Marina del Rey, CA, USA
3. Department of Psychiatry, Yale University, School of Medicine, New Haven, CT, USA
4. Genomics Computing Center, University of Texas at Rio Grande Valley, TX, USA
5. University of Texas Health Science Center at Saint Antonio, TX, USA
6. National Institute of Mental Health, Bethesda, MD, USA
7. Center for Biomedical Imaging, Department of Radiology, New York University School of Medicine, NY, USA
8. Department of Statistics, University of Warwick, Coventry, CV47AL, UK

* Corresponding Author: pkochunov@mprc.umaryland.edu

Maryland Psychiatry Research Center, Department of Psychiatry
University of Maryland School of Medicine, Baltimore, MD, USA
Phone: (410) 402-6110; Fax: (410) 402-6778

Abstract

Background.

We measured and compared heritability estimates for measures of functional brain connectivity extracted using the Enhancing Neuroimaging Genetics through Meta-Analysis (ENIGMA) rsfMRI analysis pipeline in two cohorts: the GOBS (Genetics of Brain Structure) cohort and the HCP (the Human Connectome Project) cohort. These two cohorts were assessed using conventional (GOBS) and advanced (HCP) rsfMRI protocols, offering a test case for harmonization of rsfMRI phenotypes, and to determine measures that show consistent heritability for in-depth genome-wide analysis.

Methods: The GOBS cohort consisted of 334 Mexican-American individuals (124M/210F, average age= 47.9 ± 13.2 years) from 29 extended pedigrees (average family size = 9 people; range 5-32). The GOBS rsfMRI data was collected using a 7.5-minute acquisition sequence (spatial resolution= $1.72 \times 1.72 \times 3$ mm³). The HCP cohort consisted of 518 twins and family members (240M/278F; average age= 28.7 ± 3.7 years). rsfMRI data was collected using 28.8-minute sequence (spatial resolution= $2 \times 2 \times 2$ mm³).

We used the single-modality ENIGMA rsfMRI preprocessing pipeline to estimate heritability values for measures from twenty major functional networks, using (1) seed-based connectivity and (2) dual regression approaches.

Results: Heritability values of 20-40% were observed across both cohorts, with a significant positive correlation between heritability estimates across two cohorts.

Discussion: The similarity in heritability estimates for resting state connectivity measurements suggests that the additive genetic contribution to functional connectivity is robustly detectable across populations and imaging acquisition parameters. The overarching genetic influence, and means to consistently detect it, provides an opportunity to define a common genetic search space for future gene discovery studies.

Key words: functional connectivity, heritable, seed-based connectivity

Introduction

Resting state functional MRI (rsfMRI) connectivity analysis takes advantage of temporal coherence in low-frequency blood oxygenation level-dependent fluctuations, when the brain is not engaged in a goal-directed activity^{1,2}. This activity is synchronized across interconnected brain regions and may be used to link them into functional networks¹⁻⁴. Functional networks identified during the resting state are also detectable when the brain is engaged in cognitive activities. They may also be derived through independent component analysis of brain activation maps, such as these stored in the BrainMap, the largest database (over 100,000) of functional imaging studies². These functional networks are even stable enough to be detectable to some extent when a person is asleep, in a coma, or under anesthesia, and are present in infants and in non-human primates⁵⁻⁸. The stability and reproducible structure of functional networks suggests that they are a fundamental property of the brain, making it of interest to what extent individual variance depends on genetics versus other factors. To begin to study genetic influences on functional connectivity metrics, we examined and compared heritability estimates of resting state phenotypes in two independent genetically-informed cohorts collected using two familial study designs (family and twin-siblings) and conventional and state-of-the-art fMRI approaches.

Genetic analyses of rsfMRI phenotypes can be challenging due to limitations in statistical power and methodological differences in the available analysis approaches. One way to improve statistical power and consistency of the outcomes is by pooling data from multiple cohorts. As has been noted for other phenotypes from structure MRI and diffusion MRI, very large, highly powered and representative samples are difficult to collect at a single site^{9,10}, although there are some notable exceptions, e.g. the UK Biobank¹¹. Multi-site studies can collect larger and more

representative samples but require pre-processing steps to address site-specific sources of methodological variance. The ENIGMA consortium developed an rsfMRI analysis pipeline to perform consistent analysis and extraction of resting state connectivity measures across data collected using diverse protocols [7]. Here, we used this pipeline to (i) replicate findings in the first report that demonstrated significant additive genetic contribution to the inter-subject variance in the default mode network using the original (N=334) Genetics of Brain Structure (GOBS) cohort ¹²; (ii) extend this analysis to other resting state networks and (iii) replicate these findings in an independent dataset from the Human Connectome Project (HCP; [11]). The motivation for this work is to show that genetic effects on resting state connectivity measures are robust enough to serve as targets for cross-site discovery of genetic variants that affect cerebral connectivity. A key milestone in this quest is to determine resting state connectivity measures that are reliable and consistently heritable regardless of the population and/or data collection protocols.

The ENIGMA rsfMRI pipeline differs from other pipelines in two respects. Many fMRI analysis pipelines require a structural T1-weighted (T1w) brain MRI scan to regress out signal measured in the cerebrospinal fluid (CSF) and cerebral white matter and for registration of all data to a common atlas space ^{13, 14}. In the spirit of ENIGMA, this pipeline is a single-modality and uses a deformable template created from 1,100 individual images provided by ENIGMA sites to incorporate and compensate for shape distortions common to fMRI images¹⁵. This alleviates potential pitfalls of site-to-site variance in the quality of T1w data and coregistration biases that may influence extraction of rsfMRI phenotypes. Clearly both approaches are possible, and the current approach offers a reasonable and feasible approach to test and apply across sites.

Another notable difference is that the ENIGMA rsfMRI pipeline uses a noise reduction technique based on the Marchenko-Pastur Principal Component Analysis (MP-PCA), which is included to improve signal-to-noise ratio (SNR). MP-PCA-based denoising reduces signal fluctuations rooted in thermal noise and tends to increase the tSNR without altering the spatial resolution of the data. This ability to suppress thermal noise is based on data redundancy in the PCA domain, using universal properties of the eigenspectrum of random covariance matrices ¹⁶. The advantages of improving SNR using an MP-PCA approach has already been demonstrated for multi-site analyses of diffusion MRI data. In addition, the spatial maps of the noise derived from this approach may serve as important QA variable to identify regional variations in the signal due to non-linearity in RF-receiving system or other scanner hardware problems.

Additive genetic effects on brain metrics can be conveniently detected and estimated by modeling the degree of relatedness across individuals when studying the variance in a database of brain scans. First, we computed heritability measures from two commonly used familial study designs: GOBS subjects were recruited from an extended pedigree, and HCP participants were recruited from a twin/siblings registry. To examine some alternative metrics, we used two complementary measures of functional connectivity commonly used in brain mapping research: region-based (or “seed”-based) analysis, and dual regression. In the first approach, the connectivity strength is estimated based on the degree of covariance in the signal measured from two or more regions. In the second approach, the “group-wise-average” trend is regressed from the data, yielding a statistical inference on how individual subjects differ from the group average. To reduce the biases inherent in having to extract resting state networks from different cohorts, we used the pattern derived through the meta-analysis of functional activations stored in the

BrainMap database ². Overall, similarity in the heritability measurements across two diverse cohorts is helpful to offer further evidence for the suitability of the ENIGMA rsfMRI protocol and connectivity measures for more in-depth multi-site genetic analyses of cerebral functional connectivity.

Methods and Materials

Study subjects and imaging protocols:

We performed analyses in two independently collected rsfMRI datasets: GOBS and HCP, detailed below.

GOBS (Genetics of Brain Structure and Function study)

This cohort consisted of 334 Mexican-American individuals (124M/210F, age: 47.9±13.2 years) from 29 extended pedigrees (average family size, 9 people; range 5-32) who participated in the Genetics of Brain Structure and Function study ¹². Individuals were selected from the community as part of a large family epidemiological study focused on the San Antonio, TX region. Individuals with a history of neurological illness, stroke, or other major neurological events were excluded, as were people with brain MRI contraindications. All participants provided written informed consent on forms approved by the institutional review board at the University of Texas Health Science Center San Antonio (UTHSCSA).

All imaging was performed at the Research Imaging Institute, UTHSCSA, on a Siemens 3 T Trio scanner, using a multichannel phased array head coil. Whole-brain, resting-state functional imaging was performed using a gradient-echo echo planar imaging (EPI) sequence sensitive to the BOLD effect. The acquisition parameters were: repetition and echo times

TR/TE=3000/30 ms, spatial resolution= $1.72 \times 1.72 \times 3 \text{ mm}^3$, flip angle=90 degrees. The resting-state protocol included 43 slices acquired parallel to the sagittal plane containing the anterior and posterior commissures; the total scan time was 7.5 minute.

HCP (Human Connectome Project)

HCP cohort consisted of 518 participants (240M/278F, average age 28.7 ± 3.7) from the Human Connectome Project (HCP) dataset, released in March 2017. Participants were recruited from the Missouri Family and Twin Registry¹⁷. All HCP participants were from young adult sibships of average size 3–4 that included a monozygotic or dizygotic twin pair and (where available) their non-twin siblings. Subjects ranged in age from 22 to 37 years. This age range corresponds to a period after neurodevelopment is largely completed and before the typical age of onset of neurodegenerative changes. The inclusion and exclusion criteria are detailed elsewhere¹⁷. The HCP subjects are healthy young adults within a restricted age range and free from major psychiatric or neurological illnesses^{18, 19}. All subjects provided written informed consent on forms approved by the Institutional Review Board of Washington University in St Louis.

All HCP subjects are scanned on a customized Siemens 3 T “Connectome Skyra” scanner at Washington University in St. Louis, using a standard 32-channel Siemens receive head coil. RsfMRI data consisted of two runs in one session. Within a session, oblique axial acquisitions alternated between phase encoding in a right-to-left direction in one run and phase encoding in a left-to-right direction in the other run. Resting state images were collected using a gradient-echo echo planar imaging (EPI) sequence. The acquisition parameters were: TR/TE=720 and 33.1 ms, flip angle=52 degrees, field of view (FOV)= $208 \times 180 \text{ mm}$, matrix= 104×90 , 2.0 mm isotropic

voxels, 72 axial slices, multiband factor=8; scan time was 28.8 minute.

Functional Image Analysis

ENIGMA resting state analysis. ENIGMA developed a single-modality resting state analysis pipeline¹⁵ by implementing it in the Analysis of Functional NeuroImages (AFNI) software²⁰ (**Figure 1**). It includes the application of principal components analysis (PCA)-based denoising^{16, 21}. The denoising is the first step in this analysis pipeline to improve signal-to noise ratio (SNR) and temporal SNR (tSNR) properties of the time series data¹⁵, without losing image spatial resolution, and avoids introducing of additional partial volume effects that complicate further analyses. The MP-PCA approach does not alter the resting state network activation patterns, whereas spatial smoothing using a Gaussian kernel leads to partial voxel averaging, spreading the activations across gray and white matter regions and removing smaller nodes. Finally, the noise-maps produced by the MP-PCA approach provide valuable information for quality control - deviations from the expected uniform pattern of thermal noise, or one that slowly varies in space, may indicate problems with the coil or other scanner hardware.

In the next step, supplementary data, if provided, is used to correct spatial distortions associated with long-TE gradient echo imaging. Two available corrections are the gradient-echo ‘fieldmap’ or the reversed-gradient approach. Here, we implemented the spatial distortion corrections in the HCP dataset but distortion correction data was not collected in GOBS dataset. In the next step, a transformation is computed registering the base volume to the ENIGMA EPI template that was derived from 1,100 datasets collected across 22 sites¹⁵ to develop a spatial template and spatial atlas. This atlas has a dual purpose: it is used for regression of the global signal, but it also offers a common anatomical spatial reference frame. Next, correction for head

motion is performed by registering each functional volume to the volume with the minimum outlier fraction (suggesting it has little motion), where each transformation is concatenated with the transformation to standard space, to avoid unnecessary interpolation. Nuisance variables such as the linear trend, 6 motion parameters (3 rotational and 3 translational directions), their 6 temporal derivatives (rate of change in rotational and translational motion) and time courses from the local white matter and cerebrospinal fluid (CSF) from lateral ventricles are modeled using multiple linear regression analysis, which were then removed as regressors of no interest. Time points with excessive motion (> 0.2 mm), estimated as the magnitude of displacement from one time point to the next, including neighboring time points and outlier voxels fraction (> 0.1) are censored from statistical analysis. Images were spatially normalized to the ENIGMA EPI template in Montreal Neurological Institute (MNI) standard space for group analysis.

Functional connectivity analysis

Resting state network templates were defined based on the probabilistic regions of interest (ROIs) from 20-component analysis of the BrainMap activation database and resting fMRI dataset². We defined the binary masks of the resting state template regions from auditory network (AN), attention network (AttN), default mode network (DMN), executive control network (ECN), fronto-parietal network (FPN), salience network (SN), sensorimotor network (SMN), and visual network (VN) (**Figure 2**). Mean time series were extracted from the seed regions of each network and connectivity maps corresponding to each seed region were obtained by assessing correlations along the time series for different regions. Next, Fisher's r -to- z transformations were applied to obtain a normal distribution. We calculated seed-based functional connectivity values between seed regions in each network and performed heritability

calculation. Furthermore, we performed dual regression analysis for these all network template ROIs, and calculated the functional connectivity measures and hence heritability estimates on both datasets. (The same GOBS dataset was used in a prior study by David Glahn and colleagues¹²). In the case of dual regression, for the given network template ROIs, we computed the average single time series from the preprocessed data for each ROI, and obtained the average time series for the given network from all subjects, and then averaged these to obtain an average time series that represents the group average time trend for the corresponding network. The group average time trend was then regressed out from each subject's data, before calculating the functional connectivity values between regions.

Heritability estimation

For the heritability estimations, we used the variance components method, as implemented in the Sequential Oligogenic Linkage Analysis Routines (SOLAR) Eclipse software package (http://www.nitrc.org/projects/se_linux)²². SOLAR uses maximum likelihood variance decomposition methods, extensions of the strategy developed by Amos and colleagues²³. The covariance matrix Ω for a pedigree is given by: $\Omega = 2\Phi\sigma_g^2 + I\sigma_e^2$, where σ_g^2 is the genetic variance due to the additive genetic factors, Φ is the kinship matrix representing the pair-wise kinship coefficients among all individuals, σ_e^2 is the variance due to individual — unique environmental effects and measurement error, and I is an identity matrix (under the assumption that all environmental effects are uncorrelated among family members). Narrow sense heritability is defined as the fraction of phenotypic variance σ_p^2 attributable to additive genetic factors,

$$h^2 = \frac{\sigma_g^2}{\sigma_p^2} \quad (1)$$

The variance parameters are estimated by comparing the observed phenotypic covariance matrix with the covariance matrix predicted by kinship²². Significance of the heritability estimate is tested by comparing the likelihood of the model in which σ_g^2 is constrained to zero with that of a model in which σ_g^2 is estimated. Twice the difference between the log-likelihoods of these models yields a test statistic, which is asymptotically distributed as a 1/2:1/2 mixture of χ^2 variables with 1 degree-of-freedom and a point mass at zero. Prior to the heritability estimation, phenotype values from each dataset were adjusted for covariates including sex, age, age², age²×sex interaction, and age²×sex interaction. Inverse Gaussian transformation was also applied to ensure normality of the distribution. Outputs from SOLAR include the heritability estimate (h^2), the significance value (p), and the standard error for each trait (SE).

Results

Seed-based analysis.

Heritability of seed-based connectivity phenotypes for both cohorts are summarized in **Table 1**. We replicated the significant heritability for default mode network (DMN) functional connectivity from the posterior cingulate/precuneus to bilateral temporal-parietal regions ($h^2=34\%$, $p=0.014$) and ventromedial frontal cortex ($h^2=35\%$, $p=0.014$) in the GOBS dataset. We further replicated significant heritability of these phenotypes, in the HCP dataset. Both datasets showed the significantly heritable functional connectivity between the fronto-parietal network nodes. In case of the attention network, significant heritable functional connectivity was found between right middle frontal gyrus and superior parietal lobule, for both datasets. The right

and left motor cortices are characterized by the significantly heritable functional connections for both datasets. Heritability estimates in these and other networks showed a similar pattern of genetic control in both the GOBS and the HCP with greater evidence for statistical significance (i.e., lower p -values) observed in the HCP subjects.

Dual regression analysis.

Heritability of dual-regression-based connectivity phenotypes for both cohorts are summarized in **Table 2**. The connectivity values that were significantly heritable in the seed based approach were also significantly heritable in the dual regression analysis approach. For example, in the GOBS dataset, connectivity values for the DMN ROIs were significantly heritable from posterior cingulate/precuneus to bilateral temporal-parietal regions ($h^2=31\%$, $p=0.027$) and ventromedial frontal cortex ($h^2=25\%$, $p=0.038$) (**Table 2**). The connection from bilateral temporal-parietal regions to posterior cingulate/precuneus was likewise significantly heritable ($h^2=26\%$, $p=0.035$). The HCP dataset showed the greater evidence of statistical significance (heritability from posterior cingulate/precuneus to bilateral temporal-parietal regions; $h^2=31\%$, $p=4.0 \times 10^{-8}$ and from bilateral temporal-parietal regions to posterior cingulate/precuneus; $h^2=30\%$, $p=3.8 \times 10^{-8}$). Heritability estimates in other networks showed a similar pattern of genetic control in both datasets. We found some additional significantly heritable functional connections in the dual regression analysis compared to the seed based analysis approach for both [datasets](#).

Comparison of GOBS and HCP heritability measurements.

Heritability estimates for functional connectivity measures in the GOBS cohorts were plotted versus heritability estimates for these in the HCP cohorts for seed-based and dual

regression (**Figures 3 and 4** respectively). The lines represent the result of the linear correlation between two cohorts. There was a significant and positive correlation ($r=0.38$, $p=0.023$ for seed based approach and $r = 0.50$ $p=0.002$ for dual regression analysis approach) between heritability estimates for functional connectivity measurements in the GOBS and HCP cohorts.

Execution time

All analyses were carried out at the Washington University Center for High-Performance Computing. Dual regression analysis of GOBS resting data took about 30 min per subject/network on a modern linux server node. Analysis of HCP data consisting of $N=2,400$ fMRI volumes took about 6 hours per subject/network.

Discussion

We performed heritability analyses of the connectivity phenotypes extracted from GOBS and HCP. We used two BigData developments: the ENIGMA rsfMRI pipeline and the spatial patterns of resting state networks derived from BrainMap database. We show that about ~31% of the variance in functional connectivity may be explained by additive genetic contribution. We performed these analyses in two datasets - collected ten years apart - using a conventional and state-of-the-art connectivity protocols. We observed good consistency in the magnitude of genetic influences on resting state connectivity. Building on prior work in individual cohorts, this experiment provides direct evidence that connectivity within the DMN and other intrinsic brain networks is influenced by genetic factors. Between 20-40% of the intersubject variance in functional connectivity within functional networks was under genetic control. The level of additive genetic variance for these functional connectivity measurements were between 1/3-1/2 of the heritability estimates measured for structural phenotypes such as regional brain volumes

and diffusion characteristics of the brain but consistent with previously reported values²⁴ including heritability measurement in UK Biobank sample²⁵

This lower heritability for functional versus structural brain metrics was expected based on the reports on sensitivity of resting state connectivity to neuro-psychiatric disorders and individual physiological state and other environmental and non-genetic factors. Nonetheless, establishing heritability of resting state functional connectivity provides important information to support the use of these measures as phenotypes for genetic studies or functionally characterize genes influencing brain functions in health and illness. Showing significant heritability is necessary before these metrics they can be considered an intermediate phenotype or endophenotype for neurological or mental illnesses²⁶.

Our findings replicate prior reported heritability measurements estimated in the GOBS cohort and extend this research to harmonized analyses in the HCP subjects. The pattern of heritability showed good agreement between two cohorts collected using different imaging protocols and sample designs. Resting state connectivity is under a modest-to-moderate genetic control and this heritability can be detected in, in terms of image acquisition, in legacy and state-of-the art samples.

Relationship to Other Analysis Approaches. The ENIGMA-rsfMRI pipeline is uni-modal and is based on a population-based brain template. Prior works on rsfMRI analysis are generally multimodal and use functional and structural data²⁷. In such approaches, a spatial transformation of the functional data to the structural image for each subject is followed by nonlinear registration of the structural data to an anatomic template. The transformation field is then applied to the rsfMRI data for regressions of global connectivity signals and ROI analyses in a

common anatomical frame. Arguably, a disadvantage of this approach is that spatial distortions in rsfMRI data may prevent consistent registration with the structural data unless corrected for. Calhoun and colleagues examined the unimodal and multimodal approaches in four datasets and registering functional data to a population template led to superior registration quality, lower inter-subject variance and higher statistical significance when compared to the multimodal approach²⁷. This problem is likely to be encountered in ENIGMA studies that aggregate data collected over the past 20 years. The site-to-site variability in the quality of the T1w data and the variance in registration quality between T1w and rsfMRI images is likely to be more prominent for ENIGMA studies and therefore poses a risk of influencing the results of the overall rsfMRI analysis. Likewise, we showed that the use of a deformable template improved registration for individual EPI images, including ventricular overlap, when compared to the standard ICBM-152 template [7].

Our analysis pipeline incorporates the MP-PCA denoising algorithm that improves SNR/tSNR properties of the time series data [8,9], with no loss of spatial resolution of the image. MP-PCA removes thermal noise artifacts that can have prominent site-specific spatial patterns. In a multi-site study of diffusion MRI findings in schizophrenia, the MP-PCA approach improved the agreement in findings across three sites and improved the overall agreement with the previous meta-analytic findings in this disorder²⁸. The MP-PCA improvements were especially prominent in the HCP data. The HCP protocol pushed the limits of spatial and temporal resolution of the rsfMRI but the tSNR values in this dataset (~21) were less than the suggested minimum tSNR (30-40)²⁹. MP-PCA approach improved the average tSNR value to 40 without introduction of spatial or temporal smoothing that may have partially negated the advantages of this protocol.

The ENIGMA rsfMRI pipeline is built using NIH-supported software - AFNI - that is freely available to both non-commercial and commercial users. Free-license software opens ENIGMA collaboration to commercial entities such as pharmacological companies. It is a unimodal analysis workflow designed for consistent retrospective analyses of state-of-the-art and legacy data. The pipeline incorporates stringent quality assurance (QA) and quality control steps. It incorporates traditional QA measurements to detect and censor motion and other types artifacts that are detectable visually. It also uses novel analysis of the heterogeneity of the thermal noise within imaging volume to enable identification of more subtle artifacts such as time-and-space related variability in coil sensitivity profiles. Efforts are now ongoing to compare the performance of ENIGMA rsfMRI analysis pipeline across multiple cohorts with other rsfMRI analysis pipelines.

Acknowledgments

Support was received from NIH grants U54EB020403, U01MH108148, 2R01EB015611, R01MH112180, R01DA027680, R01MH085646.

We are grateful to Human Connectome Project and the Center for High-Performance Computing at Washington University, University of Washington St. Louis for allowing the use of their computational facility for this project.

References

1. Fox MD, Raichle ME. Spontaneous fluctuations in brain activity observed with functional magnetic resonance imaging. *Nat Rev Neurosci* 2007;8:700-711.
2. Smith SM, Fox PT, Miller KL, et al. Correspondence of the brain's functional architecture during activation and rest. *Proceedings of the National Academy of Sciences of the United States of America* 2009;106:13040-13045.
3. Biswal B, Yetkin FZ, Haughton VM, Hyde JS. Functional connectivity in the motor cortex of resting human brain using echo-planar MRI. *Magn Reson Med* 1995;34:537-541.

4. Margulies DS, Clare Kellya AM, Uddin LQ, Biswal BB, Xavier Castellanos F, Milham MP. Mapping the functional connectivity of anterior cingulate cortex. *NeuroImage* 2007;37:579-588.
5. Chen LM, Yang PF, Wang F, et al. Biophysical and neural basis of resting state functional connectivity: Evidence from non-human primates. *Magn Reson Imaging* 2017;39:71-81.
6. Mitra A, Snyder AZ, Tagliazucchi E, et al. Resting-state fMRI in sleeping infants more closely resembles adult sleep than adult wakefulness. *PLoS One* 2017;12:e0188122.
7. Wey HY, Phillips KA, McKay DR, et al. Multi-region hemispheric specialization differentiates human from nonhuman primate brain function. *Brain Struct Funct* 2014;219:2187-2194.
8. Wu TL, Wang F, Anderson AW, Chen LM, Ding Z, Gore JC. Effects of anesthesia on resting state BOLD signals in white matter of non-human primates. *Magn Reson Imaging* 2016;34:1235-1241.
9. Ioannidis JPA. How to Make More Published Research True. *PLoS Medicine* 2014;11:e1001747.
10. Jahanshad N, Kochunov P, Sprooten E, et al. Multi-site genetic analysis of diffusion images and voxelwise heritability analysis: A pilot project of the ENIGMA-DTI working group. *Neuroimage* 2013;doi:pii: S1053-8119(13)00408-4. 10.1016/j.neuroimage.2013.04.061.
11. Elliott L, Sharp K, Alfaro-Almagro F, et al. The genetic basis of human brain structure and function:
1,262 genome-wide associations found from 3,144 GWAS of multimodal brain imaging phenotypes from 9,707 UK Biobank participants. *bioRxiv* 2017.
12. Glahn DC, Winkler AM, Kochunov P, et al. Genetic control over the resting brain. *Proceedings of the National Academy of Sciences of the United States of America* 2010;107:1223-1228.
13. Jenkinson M, Beckmann CF, Behrens TE, Woolrich MW, Smith SM. FSL. *NeuroImage* 2012;62:782-790.
14. Smith SM, Jenkinson M, Woolrich MW, et al. Advances in functional and structural MR image analysis and implementation as FSL. *NeuroImage* 2004;23:S208-S219.
15. Adhikari BM, Jahanshad N, Shukla DK, et al. A resting state fMRI analysis pipeline for pooling inference across diverse cohorts: The ENIGMA rs-fMRI Protocol. *Brain imaging and behavior* 2017;(under review).
16. Veraart J, Novikov DS, Christiaens D, Ades-Aron B, Sijbers J, Fieremans E. Denoising of diffusion MRI using random matrix theory. *NeuroImage* 2016;142:394-406.
17. Van Essen DC, Smith SM, Barch DM, et al. The WU-Minn Human Connectome Project: an overview. *NeuroImage* 2013;80:62-79.
18. Edens EL, Glowinski AL, Pergadia ML, Lessov-Schlaggar CN, Bucholz KK. Nicotine Addiction in Light Smoking African American Mothers. *J Addict Med* 2010;4:55-60.
19. Sartor CE, McCutcheon VV, Pommer NE, et al. Common genetic and environmental contributions to post-traumatic stress disorder and alcohol dependence in young women. *Psychological medicine* 2011;41:1497-1505.

20. Cox RW. AFNI: software for analysis and visualization of functional magnetic resonance neuroimages. *Comput Biomed Res* 1996;29:162-173.
21. Veraart J, Fieremans E, Novikov DS. Diffusion MRI noise mapping using random matrix theory. *Magn Reson Med* 2016;76:1582-1593.
22. Almasy L, Blangero J. Multipoint Quantitative-Trait Linkage Analysis in General Pedigrees. *Am J Hum Genet* 1998;62:1198-1211.
23. Amos CI. Robust variance-components approach for assessing genetic linkage in pedigrees. *Am J Hum Genet* 1994;54:535-543.
24. Glahn D, Winkler A, Kochunov P, et al. Genetic control over the resting brain. *Proc Natl Acad Sci U S A* 2010;107:1223-1228.
25. Bycroft C, Freeman C, Petkova D, et al. Genome-wide genetic data on ~500,000 UK Biobank participants. *bioRxiv* 2017.
26. Glahn DC, Curran JE, Winkler AM, et al. High Dimensional Endophenotype Ranking in the Search for Major Depression Risk Genes. *Biol Psychiatry* 2012;71:6-14.
27. Calhoun VD, Wager TD, Krishnan A, et al. The impact of T1 versus EPI spatial normalization templates for fMRI data analyses. *Human Brain Mapping* 2017;38:5331-5342.
28. Kochunov P, Dickie EW, Viviano JD, et al. Integration of routine QA data into mega-analysis may improve quality and sensitivity of multisite diffusion tensor imaging studies. *Hum Brain Mapp* 2017.
29. Murphy K, Bodurka J, Bandettini PA. How long to scan? The relationship between fMRI temporal signal to noise and necessary scan duration. *Neuroimage* 2007;34:565-574.

Figure Captions:

Figure 1. Flowchart of ENIGMA rsfMRI analysis pipeline.

Figure 2. Resting state network template ROIs based on the BrainMap activation database and resting fMRI dataset [4]. Here, L=left, R=right, in (a) a_1/a_2 =left/right primary and association auditory cortices, in (b) r_1 =posterior cingulate/precuneus, r_2 =bilateral temporal-parietal regions and, r_3 =ventromedial frontal cortex, in (c) f_1/f_2 =left/right frontal area and p_1/p_2 =left/right parietal area, in (d) m_1/m_3 =left/right motor area and m_2 =supplementary motor area, in (e) v_1 =medial visual areas, v_2 =occipital visual areas, and v_3 =lateral visual areas, in (f) r_1 =anterior cingulate cortex and r_2 =bilateral medial frontal gyrus, in (g) r_1 =anterior cingulate cortex and r_2/r_3 =left/right insula, in (h) f_1/f_2 =left/right middle frontal gyrus and p_1/p_2 =left/right superior parietal lobule.

Figure 3. Heritability estimates for functional connectivity measured in the GOBS are presented as a scatter versus heritability estimates calculated in the HCP cohorts using seed-based analysis approach. The line represents the result of the linear correlation between two cohorts that reported a positive and significant correlation, $r = 0.378$, $p=0.023$.

Figure 4. Heritability estimates for functional connectivity measured in the GOBS are presented as a scatter versus heritability estimates calculated in the HCP cohorts using dual regression analysis approach. The line represents the result of the linear correlation between two cohorts that reported a positive and significant correlation, $r = 0.498$, $p=0.002$.

Table captions:

Table 1. Heritability estimates for measures derived from resting state networks (RSNs) from seed-based analysis approach. *Blue bolded figures are significant at 5% false discovery rate (FDR). Regions are based off of Figure 2. #Estimated heritability, h^2 (SE). Abbreviations: GOBS=Genetic of Brain Structure and Function study, HCP=Human Connectome Project.

Table 2. Heritability estimates for measures derived from resting state networks (RSNs) from dual regression analysis approach. *Blue bolded figures are significant at 5% FDR. Regions are based off of Figure 2. #Estimated heritability, h^2 (SE). Abbreviations: GOBS=Genetic of Brain Structure and Function study, HCP=Human Connectome Project.

Table 1

Network	Regions*	GOBS (N=334)		HCP (N=518)	
		Heritability [#]	p-value	Heritability [#]	p-value
Auditory network (AN)	a ₁ -a ₂	0.12 (0.16)	0.209	0.05 (0.09)	0.275
	a ₂ -a ₁	0.05 (0.14)	0.356	0.05 (0.08)	0.260
Attention network (AttN)	f ₁ -p ₁	0.20 (0.12)	0.031	0.10 (0.15)	0.288
	p ₁ -f ₁	0.21 (0.12)	0.024	0.08 (0.11)	0.213
	f ₂ -p ₂	0.32 (0.12)	0.001	0.27 (0.14)	0.010
	p ₂ -f ₂	0.31 (0.12)	0.002	0.32 (0.14)	0.005
Default mode network (DMN)	r ₁ -r ₂	0.34 (0.12)	0.007	0.27 (0.09)	1.0×10^{-7}
	r ₂ -r ₃	0.0 (0.12)	0.500	0.14 (0.09)	0.008
	r ₃ -r ₁	0.09 (0.15)	0.276	0.15 (0.11)	0.025
	r ₂ -r ₁	0.09 (0.13)	0.244	0.27 (0.09)	4.6×10^{-8}
	r ₃ -r ₂	0.0 (0.20)	0.500	0.23 (0.12)	0.002
	r ₁ -r ₃	0.35 (0.13)	0.007	0.09 (0.1)	0.120
Executive control network (ECN)	r ₁ -r ₂	0.17 (0.14)	0.088	0.17 (0.11)	0.023
	r ₂ -r ₁	0.23 (0.12)	0.024	0.23 (0.11)	0.003
Fronto-parietal network (FPN)	f ₁ -p ₁	0.14 (0.14)	0.149	0.16 (0.11)	0.019
	p ₁ -f ₁	0.13 (0.14)	0.169	0.16 (0.11)	0.018
	f ₂ -p ₂	0.31 (0.13)	0.010	0.19 (0.14)	0.034
	p ₂ -f ₂	0.29 (0.15)	0.025	0.27 (0.14)	0.042
	r ₁ -r ₂	0.20 (0.13)	0.062	0.07 (0.09)	0.121
	r ₂ -r ₃	0.24 (0.10)	0.015	0.25 (0.11)	0.002
	r ₃ -r ₁	0.00 (0.5)	0.5	0.13 (0.08)	0.005

Saliency network (SN)	r ₂ -r ₁	0.16 (0.12)	0.084	0.20 (0.11)	0.002
	r ₃ -r ₂	0.18 (0.12)	0.049	0.31 (0.12)	3.8×10⁻⁴
	r ₁ -r ₃	0.00 (0.5)	0.5	0.05 (0.06)	0.142
Sensorimotor network (SMN)	m ₁ -m ₂	0.09 (0.14)	0.255	0.29 (0.15)	0.017
	m ₂ -m ₃	0.00 (0.5)	0.500	0.14 (0.12)	0.113
	m ₃ -m ₁	0.32 (0.20)	0.041	0.27 (0.14)	0.009
	m ₂ -m ₁	0.06 (0.12)	0.302	0.00 (0.5)	0.5
	m ₃ -m ₂	0.00 (0.5)	0.500	0.15 (0.13)	0.108
	m ₁ -m ₃	0.32 (0.20)	0.045	0.25 (0.13)	0.008
Visual network (VN)	v ₁ -v ₂	0.21 (0.15)	0.062	0.14 (0.09)	0.021
	v ₂ -v ₃	0.36 (0.14)	0.004	0.17 (0.11)	0.029
	v ₃ -v ₁	0.12 (0.14)	0.168	0.03 (0.04)	0.191
	v ₂ -v ₁	0.32 (0.15)	0.008	0.13 (0.09)	0.042
	v ₃ -v ₂	0.13 (0.14)	0.161	0.15 (0.09)	0.040
	v ₁ -v ₃	0.17 (0.14)	0.100	0.06 (0.05)	0.060

Table 2

		GOBS (N=334)		HCP (N=518)	
Network	Regions*	Heritability [#]	<i>p</i> -value	Heritability [#]	<i>p</i> -value
Auditory network (AN)	a ₁ -a ₂	0.07 (0.13)	0.479	0.07 (0.09)	0.188
	a ₂ -a ₁	0	0.500	0.06 (0.08)	0.221
Attention network (AttN)	f ₁ -p ₁	0.25 (0.15)	0.041	0.27 (0.15)	0.031
	p ₁ -f ₁	0.25 (0.15)	0.043	0.17 (0.13)	0.091
	f ₂ -p ₂	0.29 (0.15)	0.029	0.31 (0.13)	0.009
	p ₂ -f ₂	0.36 (0.16)	0.010	0.40 (0.12)	0.002
Default mode network (DMN)	r ₁ -r ₂	0.30 (0.16)	0.014	0.31 (0.09)	4.0×10 ⁻⁸
	r ₂ -r ₃	0	0.500	0.15 (0.09)	0.010
	r ₃ -r ₁	0.09 (0.11)	0.279	0.14 (0.10)	0.038
	r ₂ -r ₁	0.26 (0.16)	0.035	0.30 (0.09)	3.8×10 ⁻⁸
	r ₃ -r ₂	0	0.500	0.20 (0.11)	0.004
	r ₁ -r ₃	0.25 (0.17)	0.038	0.08 (0.09)	0.131
Executive control network (ECN)	r ₁ -r ₂	0.26 (0.14)	0.026	0.20 (0.12)	0.016
	r ₂ -r ₁	0.26 (0.13)	0.024	0.22 (0.10)	0.009
Fronto-parietal network (FPN)	f ₁ -p ₁	0.13 (0.14)	0.159	0.17 (0.12)	0.022
	p ₁ -f ₁	0.10 (0.15)	0.235	0.15 (0.11)	0.027
	f ₂ -p ₂	0.33 (0.14)	0.010	0.23 (0.14)	0.041
	p ₂ -f ₂	0.30 (0.16)	0.027	0.30 (0.11)	0.012
	r ₁ -r ₂	0.26 (0.15)	0.047	0.07 (0.08)	0.116
	r ₂ -r ₃	0.26 (0.16)	0.043	0.26 (0.12)	0.001

Saliency network (SN)	r_3-r_1	0.07 (0.15)	0.318	0.15 (0.09)	0.004
	r_2-r_1	0.14 (0.14)	0.160	0.20 (0.11)	0.002
	r_3-r_2	0.25 (0.14)	0.037	0.35 (0.12)	0.001
	r_1-r_3	0	0.500	0.07 (0.06)	0.099
Sensorimotor network (SMN)	m_1-m_2	0.12 (0.14)	0.179	0.30 (0.13)	0.013
	m_2-m_3	0.05 (0.18)	0.397	0.24 (0.14)	0.009
	m_3-m_1	0.37 (0.18)	0.013	0.27 (0.13)	0.008
	m_2-m_1	0.13 (0.13)	0.151	0.26 (0.14)	0.009
	m_3-m_2	0.06 (0.16)	0.352	0.16 (0.14)	0.088
	m_1-m_3	0.40 (0.15)	0.007	0.13 (0.12)	0.135
Visual network (VN)	v_1-v_2	0.25 (0.15)	0.044	0.24 (0.08)	0.006
	v_2-v_3	0.35 (0.14)	0.005	0.32 (0.11)	0.001
	v_3-v_1	0.14 (0.14)	0.135	0.04 (0.05)	0.194
	v_2-v_1	0.31 (0.11)	0.008	0.22 (0.11)	0.009
	v_3-v_2	0.16 (0.14)	0.121	0.15 (0.09)	0.044
	v_1-v_3	0.22 (0.13)	0.050	0.12 (0.06)	0.026

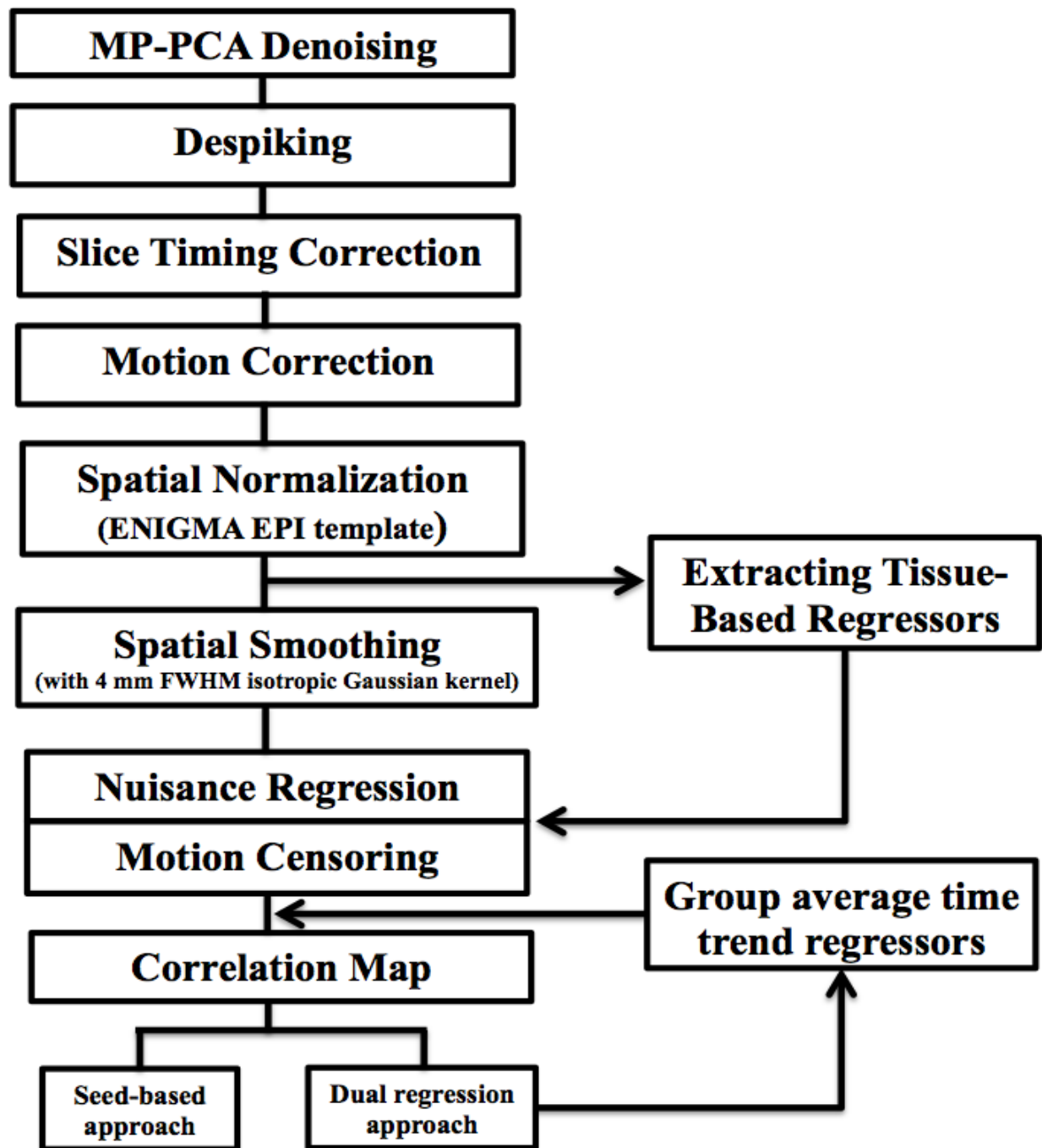


Figure 1

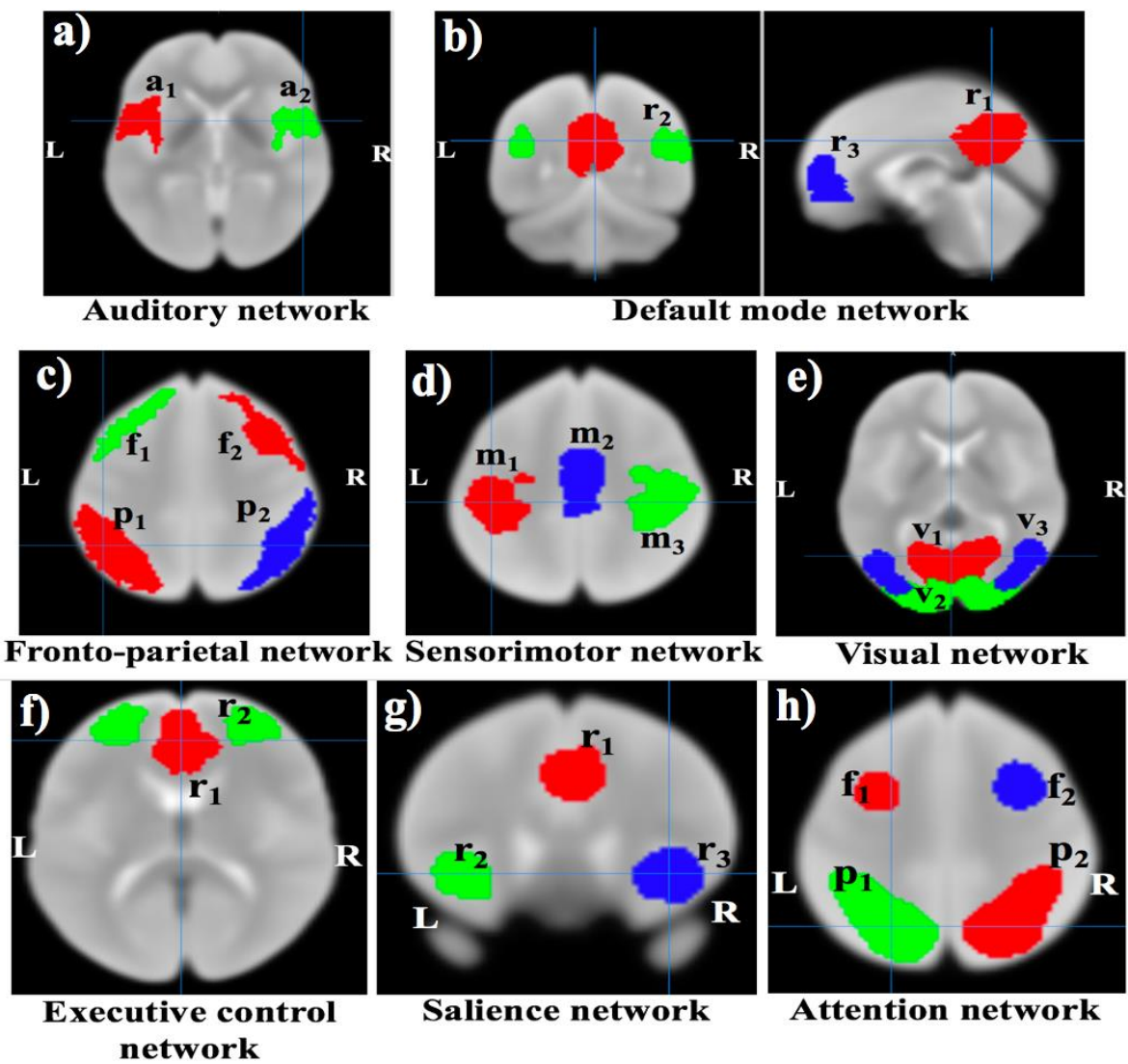


Figure 2

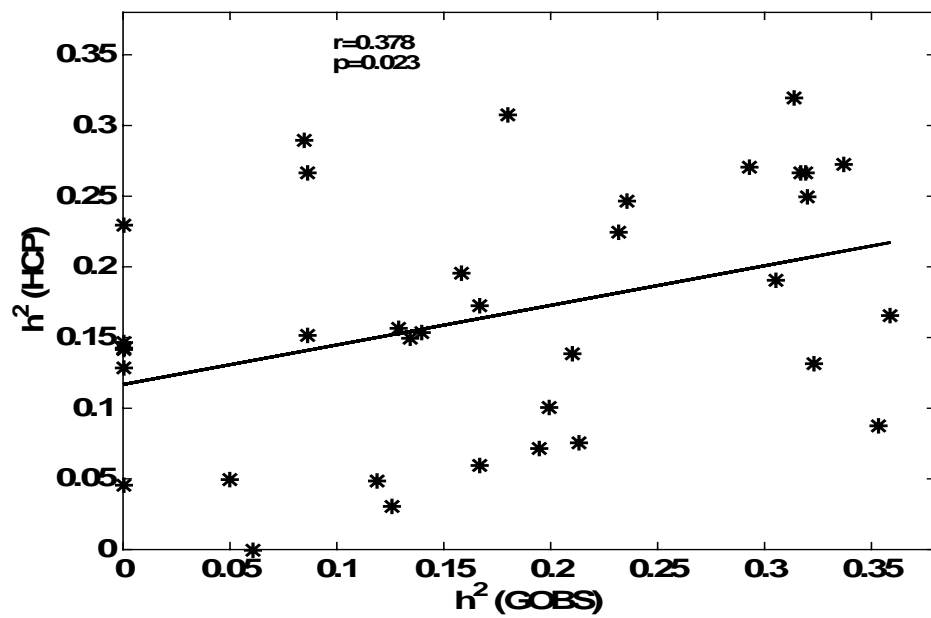


Figure 3

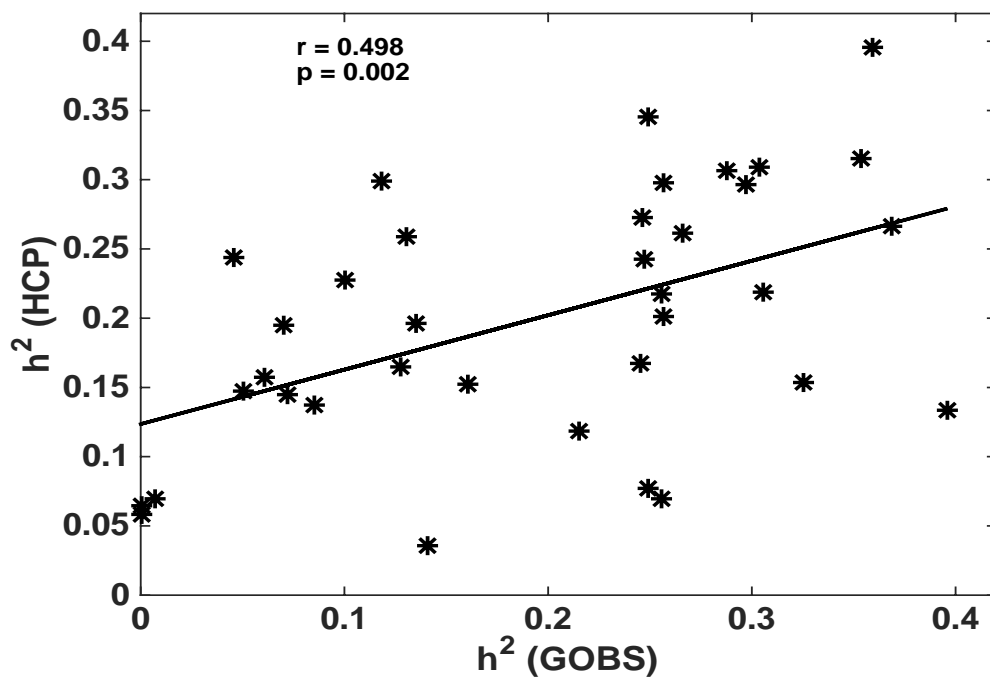


Figure 4